SEDIMENTOLOGY the journal of the International Association of Sedimentologists

Sedimentology (2011) doi: 10.1111/j.1365-3091.2011.01268.x

Bed-thickness and grain-size trends in a small-scale proglacial channel–levée system; the Carboniferous Jejenes Formation, Western Argentina: implications for turbidity current flow processes

MASON DYKSTRA*, BEN KNELLER† and JUAN-PABLO MILANA‡
*Department of Geology and Geological Engineering, 1516 Illinois St., Colorado School of Mines, Golden, CO 80401, USA (E-mail: mdykstra@mines.edu)
†Department of Geology and Petroleum Geology, University of Aberdeen, Aberdeen AB24 3UE, UK
‡CONICET and Instituto de Geología, Universidad Nacional de San Juan, San Juan, Argentina

Associate Editor – Jess Trofimovs

ABSTRACT

Preserved in Quebrada de las Lajas, near San Juan, Argentina, is an ancient subaqueous proglacial sedimentary succession that includes a small-scale (*ca* 50 m thick and *ca* 200 m wide) channel–levée system with excellent exposure of the channel axis and levée sediments. Coeval deposition of both the channel axis and the levées can be demonstrated clearly by lateral correlation of individual beds. The channel axis consists predominantly of a disorganized, pebble to boulder conglomerate with a poorly sorted matrix. The channel axis varies from 10 to 20 m wide and has a total amalgamated thickness of around 50 m. Beds fine gradationally away from the cobble–boulder conglomerates of the channel axis within a few metres, transitioning to well-organized pebble to cobble conglomerates and sandstones of the channel margin. Within 60 m outboard of the channel axis in both directions, perpendicular to the trend of the channel axis, the mean grain size of the beds in the levées is silt to fine-grained sand. Deposits in this channel–levée system are the product of both debris flows (channel axis) and co-genetic turbidity currents (channel margins and levées). Bed thicknesses in the levées increase for up to 10 to 25 m away from the channel axis, beyond which bed thicknesses decrease with increasing distance. The positions of the bed thickness maxima define the levée crests, and the thinning beds constitute the outer levée slopes. From these relationships it is clear that the levée crest migrated both away from and toward the channel axis, and varied in height above the channel axis from 4 to 5 m (undecompacted), whereas the height of the levée crest relative to the distal levée varied from 4·5 to 10 m, indicating that the channel was at times super-elevated relative to the distal levée. Bed thickness decay on the outside of the levée crest can be described quite well with a power-law function (R^2 = 0·85), whereas the thickness decay from the levée crest toward the channel axis follows a linear function (R^2 = 0·78). Grain-size changes are quite predictable from the channel margin outward, and follow logarithmic (R^2 = 0·77) or power-law (R^2 = 0·72) decay curves, either of which fit the data quite well. This study demonstrates that, in at least this case: (i) levée thickness trends can be directly related to channel-flow processes; (ii) individual bed thickness changes may control overall levée geometry; and (iii) levée and channel deposits can be coeval.

Keywords Bed thickness decay, Carboniferous, channel, channel-levée, debris-flow, deglacial, pro-glacial, turbidity current.

INTRODUCTION

The typical gull-wing cross-sectional shape of undeformed deep marine levées is thought to be caused by a rapid increase in levée thickness away from the channel margin toward the levée crest, followed outward by a decrease in thickness from the levée crest toward the distal levée (Skene *et al.*, 2002). Whether these thickness changes directly reflect changes on the bed-scale or at a larger scale is not completely clear, but some bed-scale studies (DeVries & Lindholm, 1994; Beaubouef, 2004; Kane, 2007; Kane *et al.*, 2007; Hubbard *et al.*, 2008) have shown consistent thickness decay of sandstone beds with distance from the channel margin on the outside of the inferred levée crest. Kane *et al.* (2007) rigorously examined the thickness decay of beds and bed packages on the outside of a levée crest, demonstrating that these thickness changes follow a power-law decay. Skene *et al.* (2002), however, concluded that the total thickness of submarine levées followed an exponential thinning away from their associated channel. Kane (2007) and Birman *et al.* (2009) discussed published and unpublished data showing that different decay laws exist on different regional gradients, and Birman *et al.* (2009) suggested that this is a function of the rate of entrainment of water into the currents that build the levées. Additionally, a number of workers have examined the thickness decay of deposits from experimentally generated turbidity currents in flumes, most of which exhibited exponential thickness decays (Bonnecaze *et al.*, 1993; Gladstone *et al.*, 1998; De Rooij & Dalziel, 2009; Kane *et al.*, 2010). No published work to date has addressed bed thickness and grain-size changes inside the levée crest, although due to the proximity to stronger currents, erosional complications are expected to make for a more variable thickness record than that preserved outside the levée crest (Kane & Hodgson, 2011). How levée geometry relates to event bed thickness and grain-size distributions both inside and outside of the levée crest has significant implications for the understanding of both turbidity flow processes, and for volumes and connectivity of hydrocarbon reservoirs in the subsurface (Clemenceau *et al.*, 2000). Numerical and physical modelling support the interpretation that these thickness changes occur at the individual turbidity current event level (Peakall *et al.*, 2000; Felix, 2002; Mohrig & Buttles, 2007; Birman *et al.*, 2009; Kane *et al.*, 2010) and, therefore, at the bed level. Because there are very few examples of channel–levées at outcrop where individual beds can be correlated from the channel margin to the distal levées, however, there has been very little rock data to support this hypothesis.

Additionally, it is not well-established whether or not the thickness changes in levées behave predictably between systems with different input parameters (for example, grain-size distribution, water salinities, river flood versus slump-generated turbidity currents, and channel gradient), or even within individual channel–levée systems. Presented here is a detailed analysis of the spatial distribution of bed thicknesses and grain sizes from a small palaeofjord-head system in Quebrada de las Lajas, Western Argentina.

GEOGRAPHIC AND GEOLOGICAL SETTING

The sedimentary succession described here comprises a portion of the Jejenes Formation, the fill of a small sub-basin of the Paganzo Basin (Carboniferous) which lies mainly to the north of the field area (Fernández Seveso & Tankard, 1995; Limarino *et al.*, 2002; Pazos, 2002). The exposure is in a modern valley (Quebrada de las Lajas) that exhumes a deeply incised, middle Carboniferous palaeofjord on the eastern slopes of the Sierra Chica de la Zonda, part of the Eastern Precordillera of the Andes, near San Juan, Western Argentina (Fig. 1; Dykstra *et al.*, 2006). During the late middle Carboniferous, the Quebrada de las Lajas palaeofjord was located at a latitude of approximately 60° south on the eastern side of a mountain range (or ranges), the proto-Precordillera, that separated the epicratonic Paganzo basin (a retro-arc foreland basin) from the open ocean to the west (Ramos, 1988; López-Gamundí *et al.*, 1992; Fernández Seveso & Tankard, 1995). During the mid-Carboniferous Gondwanan glaciations, a complicated network of palaeovalleys was formed in what is now the Precordillera to the Andes (Milana & Bercowski, 1990; Kneller *et al.*, 2004). Although the lithostratigraphic nomenclature differs accord-

Fig. 1. Location map of the field area. Modified from Dykstra *et al.* (2006).

ing to variability in sedimentary fill, all these palaeovalley fills are linked to a similar evolution owing to a rapid, synchronous deglaciation and the resultant eustatic rise (Kneller *et al.*, 2004; Dykstra *et al.*, 2006). The palaeofjord of Las Lajas was carved during the mid to late Carboniferous glaciations, and currently preserves over 1000 m of relief cut into the Lower Palaeozoic shelf carbonates of the San Juan Formation (Dykstra *et al.*, 2006). These rocks were already steeply dipping by the Carboniferous, having been deformed by a Late Devonian terrane accretion event, and comprised a mountain range at the time (Beresi & Bordonaro, 1985; Keller, 1999).

After deglaciation in the middle Carboniferous, the marine transgression advanced up the large fjords that dissected the elevated terrain, thereby connecting the craton with the open ocean to the west (Salfity & Gorustovich, 1983; Kneller *et al.*, 2004), and reached Quebrada de las Lajas while a valley glacier was still present in the valley head (Dykstra *et al.*, 2006). The palaeofjord was filled before, during and shortly after this marine transgression.

STRATIGRAPHIC FRAMEWORK

The palaeofjord fill is subdivided on the basis of facies, facies associations and their interpreted depositional settings into four main evolutionary stages (Figs 2 to 4; Dykstra *et al.*, 2006, 2007a).

1 Stage 1: (a) glacial ice-contact (glaciotectonically deformed), Gilbert-type deltas and subaqueous (probably lacustrine) fans; and (b) deep lacustrine or restricted marine succession including numerous channels, a channel–levée system, and mass-transport deposits (Fig. 4; the succession presented here).

2 Stage 2: postglacial marine transgressive succession, with basal chaotic mass-transport deposits and associated topographically controlled channels, incised slope channels and coherent (slide-sheet dominated) mass-transport deposits.

3 Stage 3: sheet-like turbidite sandstone bodies and large-scale, coherent mass-transport deposits.

4 Stage 4: coarse-grained subaqueous delta sheet sandstones and conglomerates, and plentiful, small-scale mass-transport deposits.

The focus of this paper is a small channel–levée system (*sensu* Damuth *et al.*, 1988) deposited during Stage 1.

LOCAL GEOLOGICAL SETTING AT DEPOSITION OF STAGE 1

During deposition of the channel–levée system, Quebrada de las Lajas was filled with brackish or fresh water, and was probably dammed at its mouth, either by a large valley glacier in front of the mountain range, or by a large terminal moraine from a former ice maximum position (Dykstra, 2005; Dykstra *et al.*, 2006). The water depth in the valley was probably a few tens of metres, based on the height of delta clinoforms a few hundred metres up-valley from the channel–levée system; sediments in the palaeovalley were transported and deposited by sediment gravity flows, primarily turbidity currents and debris flows. The overall setting was that of a laterally confined basin with a seasonal sediment supply related to summer melting of the valley glacier at its head (Dykstra, 2005; Dykstra *et al.*, 2006). Sediment was supplied axially, with the exception of sporadic local rockfalls from the palaeovalley sides. Similar to modern lacustrine or marine proglacial systems, sediment supply was probably abundant, perhaps with several metres of sediment deposited annually (Mackiewicz *et al.*, 1984; Fleisher *et al.*, 2003), resulting in very rapid progradation of a delta or outwash fan system, and rapid aggradation of the entire channel–levée system discussed here.

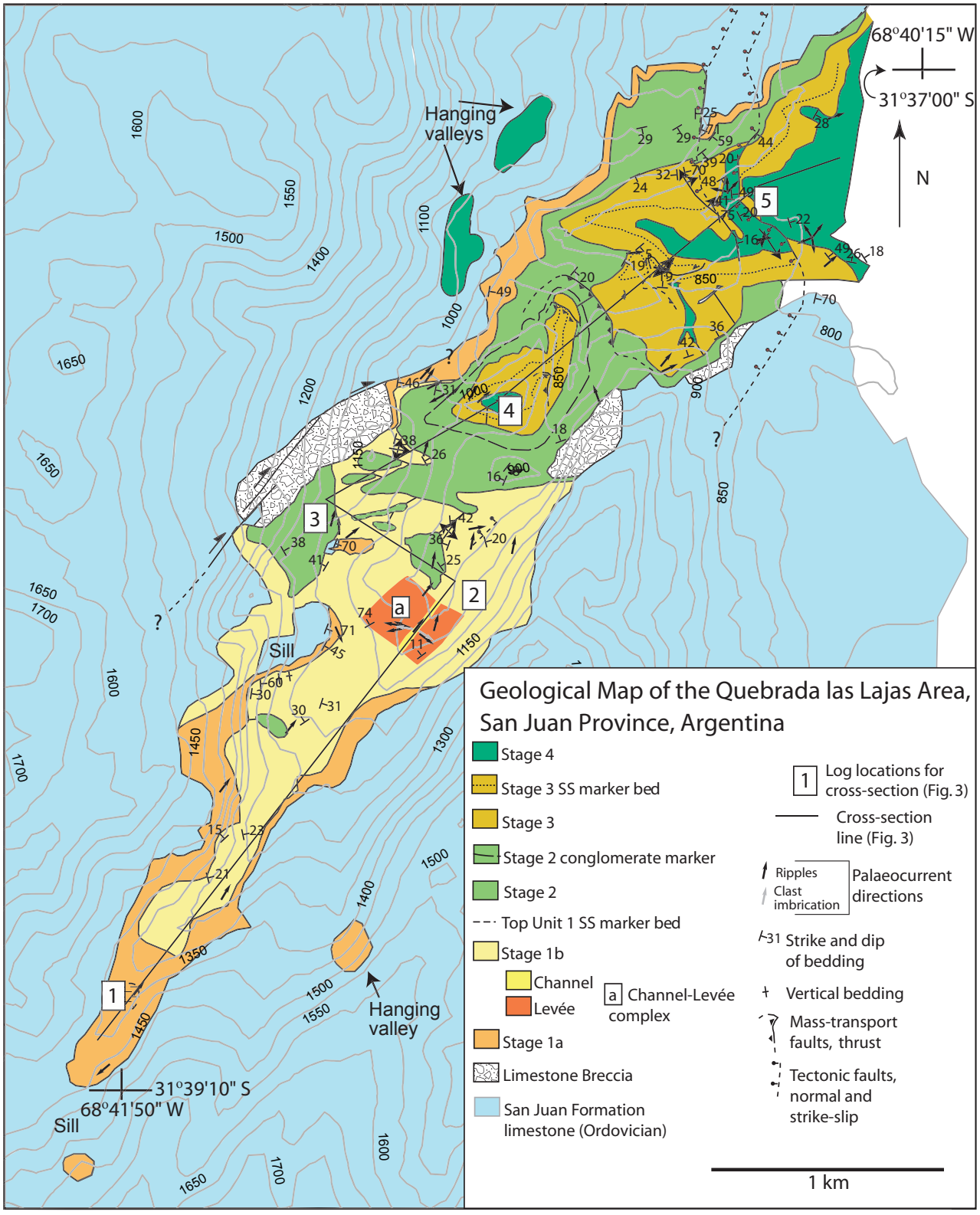

Fig. 2. Geological map of the Quebrada de las Lajas Carboniferous outcrops, showing the various units of palaeovalley fill that correspond to the evolutionary stages presented in Dykstra *et al.* (2006) and shown in Fig. 3. The Channel levée complex reported here is shown by location 'a', part of Stage 1b, when the palaeovalley still had a glacier at its head and was brackish marine or lacustrine in nature.

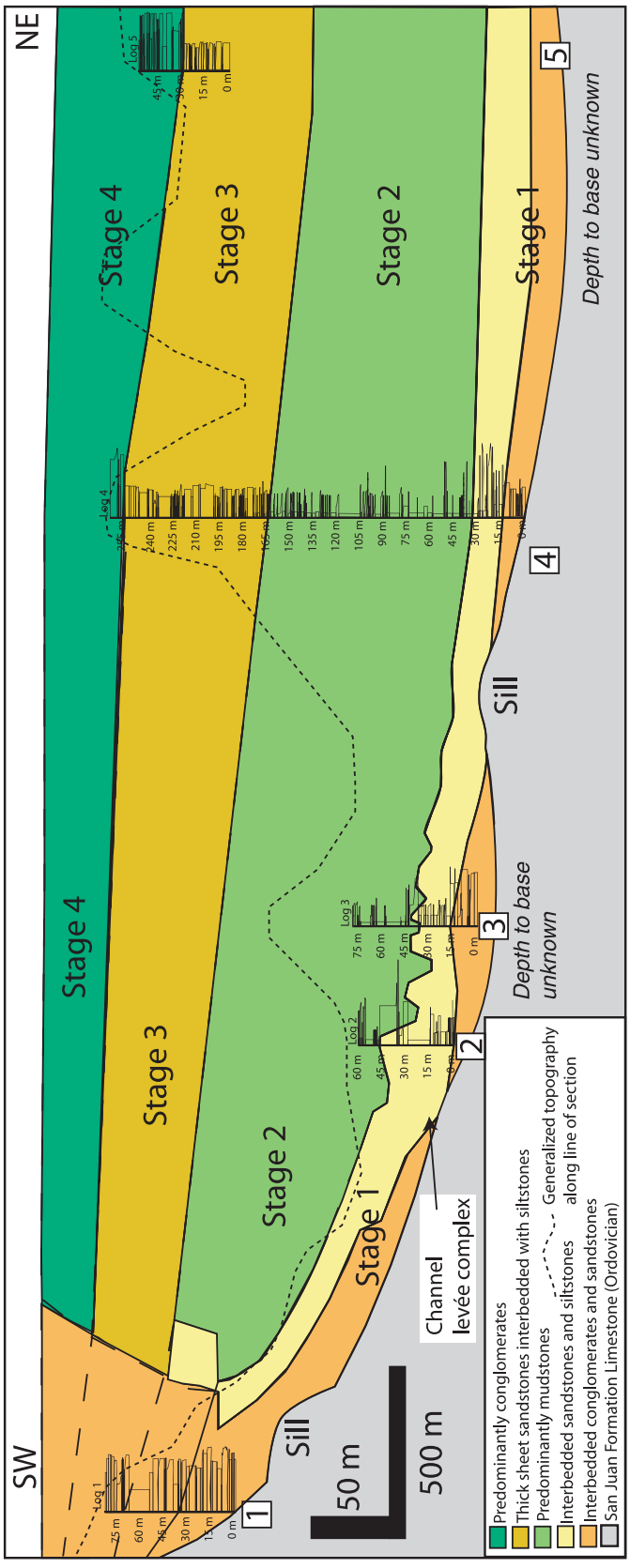

Fig. 3. Cross-section, in depositional dip section, showing the depositional units and evolutionary stages of the palaeovalley. The channel–levée system reported here is part of Stage 1. A reconstruction of this stage of the palaeovalley evolution is shown in Fig. 4A. Modified from Dykstra *et al.* (2006).

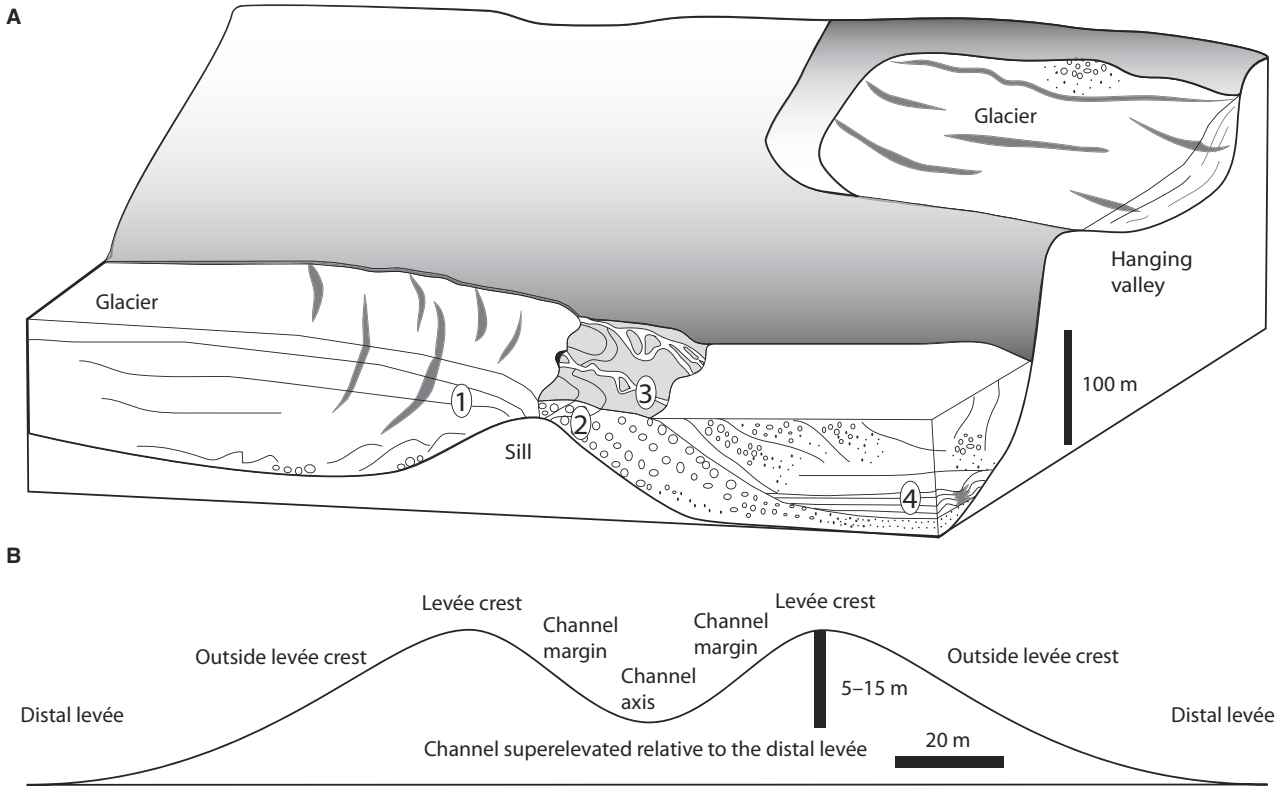

Fig. 4. (A) Palaeoenvironmental reconstruction of the valley during Stage 1 when the channel–levée system was deposited. During this stage, there was a valley glacier present up-valley from the outcrop location (1), a coarse-grained proglacial delta (2) possibly with a short fluvial topset (3), and a channel–levée system (4) in a brackish marine or lacustrine setting. Modified from Dykstra *et al.* (2006). (B) Simple cartoon cross-section of an idealized channel–levée system, showing the terminology used in this paper.

CHANNEL–LEVÉE SYSTEM

The channel–levée system described here is part of the lower to middle portion of the Stage 1 deposits (Fig. 2; Dykstra, 2005; Dykstra *et al.*, 2006). This channel–levée system consists of exposed channel axis, channel margins and levée deposits on both sides of the channel, with preserved levée crest and outer levée, each with distinct lithofacies and sedimentary structures (Figs 5 to 7). The channel–levée system was fed from an ice-contact delta a few hundred metres up-valley, which provided cold, dense, sediment-laden water directly into the fjord during the summer melt season, probably via a subglacial jet (Dykstra *et al.*, 2006, 2007a).

Channel-axis Deposits: Description

The channel axis comprises matrix-supported to clast-supported, very poorly sorted, chaotic conglomerates that vary from pebble to boulder in maximum clast size, with a principal mode in the small cobble size range and a fine to medium-grained sandstone matrix. Sedimentary structures are relatively rare, and include dewatering structures and deformation textures distinguishable where the sandstone matrix is more abundant. No clear clast fabrics are present in the channel axis. The conglomerates are highly amalgamated, with numerous erosion surfaces distinguishable on the basis of abrupt grain-size changes (Fig. 8). The channel-axis conglomerates are present in a zone approximately 10 to 20 m wide, perpendicular to the mapped trend of the channel axis (038°; Figs 2, 5, 6 and 7). These conglomerates crop out over 50 to 60 m thickness, while generally maintaining the same width. The channel-axis deposits have, overall, a very low aspect ratio (width/thickness ratio <0·2), they are vertically stacked and laterally very restricted.

Channel-axis Deposits: Interpretation

The channel axis represents the focus of energy of the channel–levée system, as evidenced by the coarse-grained nature of the deposits and numerous erosion surfaces it contains. The chaotic nature

Fig. 5. Photomosaic of the channel–levée system, showing the channel axis on the right, and correlations of the stratigraphic levels used in this study. Grain-size sample locations are shown. This view is approximately perpendicular to the trend of the channel axis looking down palaeoflow for the channel and highlights quite well the highly aggradational character of the channel–levée system. Note that many beds can clearly be traced from the channel axis, through the channel margin, over the levée crest, and into the distal levée.

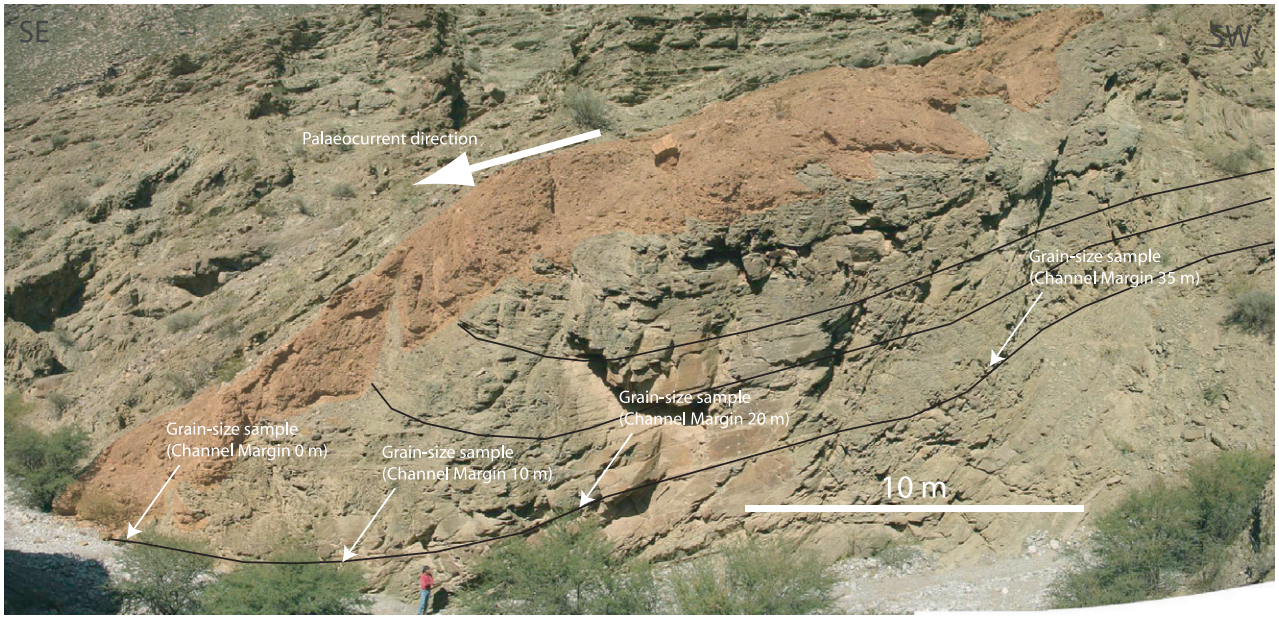

Fig. 6. Photomosaic of the channel–levée system, slightly up depositional dip from Fig. 5, showing an oblique depositional dip section of the channel axis and the levée. Grain-size sample locations are shown.

of the deposits within the channel axis suggests deposition from debris flows, although it is not clear whether these textures represent a transport regime with a plastic rheology (Iverson, 1997) or evolution from a turbulence-supported to a plastic regime during deposition. The highly aggradational character of the channel axis is clear from the very low aspect ratio of the deposits.

Channel-margin Deposits: Description

The channel margin comprises the wings of the channel-axis deposits, including the levée between the channel and the levée crest (Figs 4, 7 and 8). The deposits in this setting consist of interbeds of matrix-supported and clast-supported, often imbricated ($a_t - b_i$; *a*-axis transverse, *b*-axis inclined) and normally graded pebble to cobble conglomerates and laminated or ripple cross-laminated medium to coarse sandstones (Fig. 7). Palaeocurrent directions from clast imbrication exhibit a vector mean to 281° (n = 8) on the north-western margin of the channel, and to 123° (n = 5) on the south-eastern margin (Fig. 2). Cryptic bedding from the channel axis can be traced into very well-defined beds in the channel margin. Further from the channel axis the conglomerate interbeds either pinch out or, more commonly, fine laterally into sandstones (Figs 5 to 8). Individual beds and packages can easily be walked out from the channel margin into the distal deposits (Fig. 7), where the sandstone beds continue to fine, from coarse to medium-grained and fine-grained sand, and then progressively to silt most distally (all within about 60 m). Within *ca* 5 m from the channel-axis/channel-margin boundary, random floating pebbles and cobbles are commonly present in these sandstone beds, but are completely absent at greater distances (Fig. 8). Beds tend to thin from the channel axis into the channel margin and then thicken to a maximum value within 14 to 21 m from the channel-margin/channel-axis transition, although in some cases beds in the channel margin are erosionally truncated by axial deposits (Figs 7 and 8). Beds progressively thin beyond this maximum (Figs 7 and 9).

Channel-margin Deposits: Interpretation

The channel margin is a composite setting, representing the transition between the channel proper and the levée crest (Figs 4, 7 and 8), and thus comprises the inner levée. In this locality individual beds are traceable from the channel axis over the levée crest, although a major change in facies characterizes this transect from gravel, with a medium to coarse-grained sand matrix, to fine-grained sandstone. While chaotic deposits dominate in the channel axis, much more organized deposits characterize the channel margin up to the levée crest. Regular tractive-type clast fabrics are present in the gravels of the channel margin, suggesting that deposition from bedload dominated over direct suspension sedimentation or frictional freezing. Due to a complete absence of traction-type deposits in the

channel-axis deposits, it seems highly unlikely that these fabrics on the channel margin could be a product of reworking, (without leaving any trace of reworking in the channel axis) although that possibility cannot be ruled out completely. In addition to the clast fabrics, sedimentary structures indicative of bedload transport such as plane-bed lamination are plentiful on the inside of the levée crest. The fact that pebbles are not observed more than 5 m from the channel-axis to margin transition suggests either a rapid lateral decrease in the competence of flows, or a paucity of coarse granular material higher in the flows. However, many individual beds initially decrease then increase in thickness away from the channel axis (Fig. 7), while along the same transect exhibit a progressive decrease in both mean and maximum grain-size (Figs 5 to 8), implying a complicated depositional regime: the flows appear to have lost their competence much faster than their capacity; thus, while a clear lateral grain-size fining occurs, a discrete bed thinning then thickening occurs. Therefore, it appears that there is a change laterally from en-masse sedimentation in the channel axis to capacity-driven sedimentation at the channel margin.

Levée Sediments: Description

Outside the levée crest the levée sediments consist of <1 to 8 cm thick interbeds of sandstone and siltstone, with an overall fining and thinning away from the channel axis. Sedimentary structures in levée beds include parallel lamination, ripple cross-lamination and convolute lamination. Palaeocurrent direction indicators (primarily ripple cross-laminae) of the fine-grained sediments on the north-western margin of the channel trend toward 265° (n = 16), and on the south-eastern margin to 106° (n = 10; Figs 2 and 7).

Levée Sediments: Interpretation

Given the clear lateral facies transition from conglomerates and sandstones in the lower part of the channel margin to sandstones at the levée crest and siltstones in the distal levée, the levée was probably deposited directly via overspill from the channel and, hence, aggraded apace with the channel. The dramatic fining away from the channel axis is probably due to the large amount of topographic relief on the levées (4 to 10 m; Fig. 9), the high bedload component of these flows, and the stratified nature of turbidity currents; the topographically higher levées would have tapped higher parts of the flows, where the mean and maximum grain sizes were lower (Chough & Hesse, 1980; Kneller & Buckee, 2000). The continued fining away from the levée crest is probably due to sediment gravity-flow collapse and rapid sediment fall-out on the back of the levées as momentum was lost and the currents expanded (Normark, 1978; Kneller, 1995). The channel–levée system was highly aggradational, with little lateral movement of the channel axis, although there is a general westward migration at higher stratigraphic levels (Figs 5 to 7). The high degree of confinement of the overall palaeofjord may have been a controlling factor in this highly aggradational character, resulting in rapid aggradation on the basin floor, and thus of the pinning point of the channel profile at the channel mouth (e.g. Kneller, 2003).

BED THICKNESS TRENDS INSIDE THE LEVÉE CREST (CHANNEL MARGIN)

Bed thicknesses were measured at several different stratigraphic levels in the levée (Fig. 5), in a transect approximately perpendicular to the transport direction within the channel axis (confirmed by the mapped trend of the channel axis, and palaeocurrent directions within the levée facies). By normalizing the data using the distance from the channel-axis to margin transition to the levée crest as a characteristic horizontal length scale, and the maximum levée height for each individual stratigraphic interval as a characteristic vertical length scale, the data were reduced to a format whereby different stratigraphic levels can easily be compared. Inside the levée crest, these stratigraphic surfaces slope toward the channel axis and are only slightly deformed by syn-depositional deformation (Dykstra *et al.*, 2007b); although some folding is present in these deposits, it has been interpreted as larger scale sliding that post-dates deposition of the entire channel–levée system (Dykstra *et al.*, 2006). Bed thicknesses inside the levée crest decrease toward the channel axis in a linear fashion, both when all stratigraphic levels selected are analyzed together (Fig. 10; R^2 = 0·78), and when analyzed individually (Fig. 10; R^2 = 0·95, 0·98 and 0·77). The sensitivity of the data to decompaction was tested using simple porosity–depth curves (Bond & Kominz, 1984), assuming a burial of 1 km and initial porosities of 40% for sandstone and 45 to 60% for siltstone, scaled using the log data (Fig. 10). Decompacting

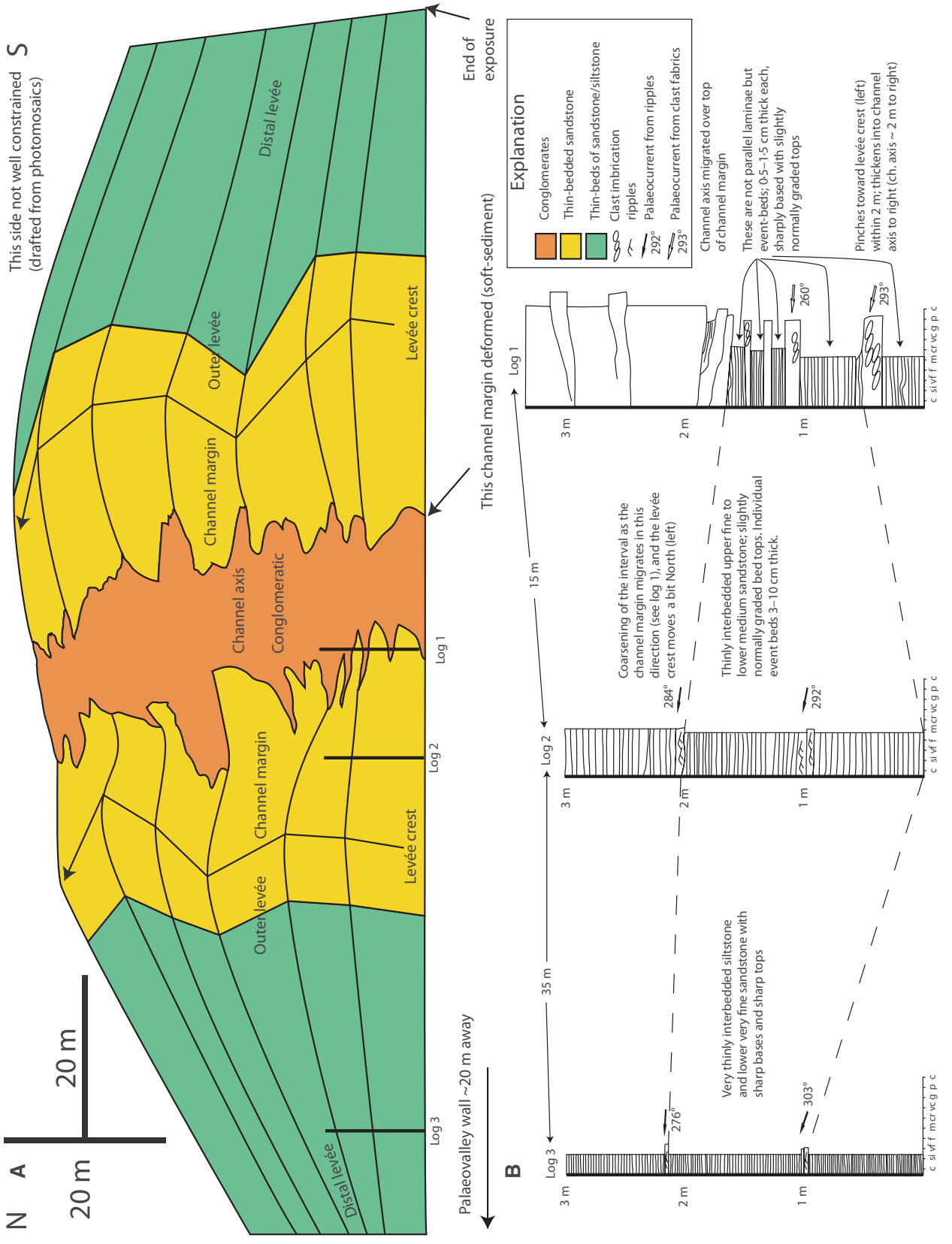

Fig. 7. (A) Cross-section of the channel–levée system flattened on the first correlatable stratum above the creek level, showing the approximate lateral distribution of facies, and a number of beds that can be correlated laterally from the channel margin to the distal levée. (B) Sedimentary logs of one of the levée levels, showing representative facies for the channel margin/axis (Log 1), the levée crest (Log 2) and the distal levée (Log 3). Correlations between logs are shown.

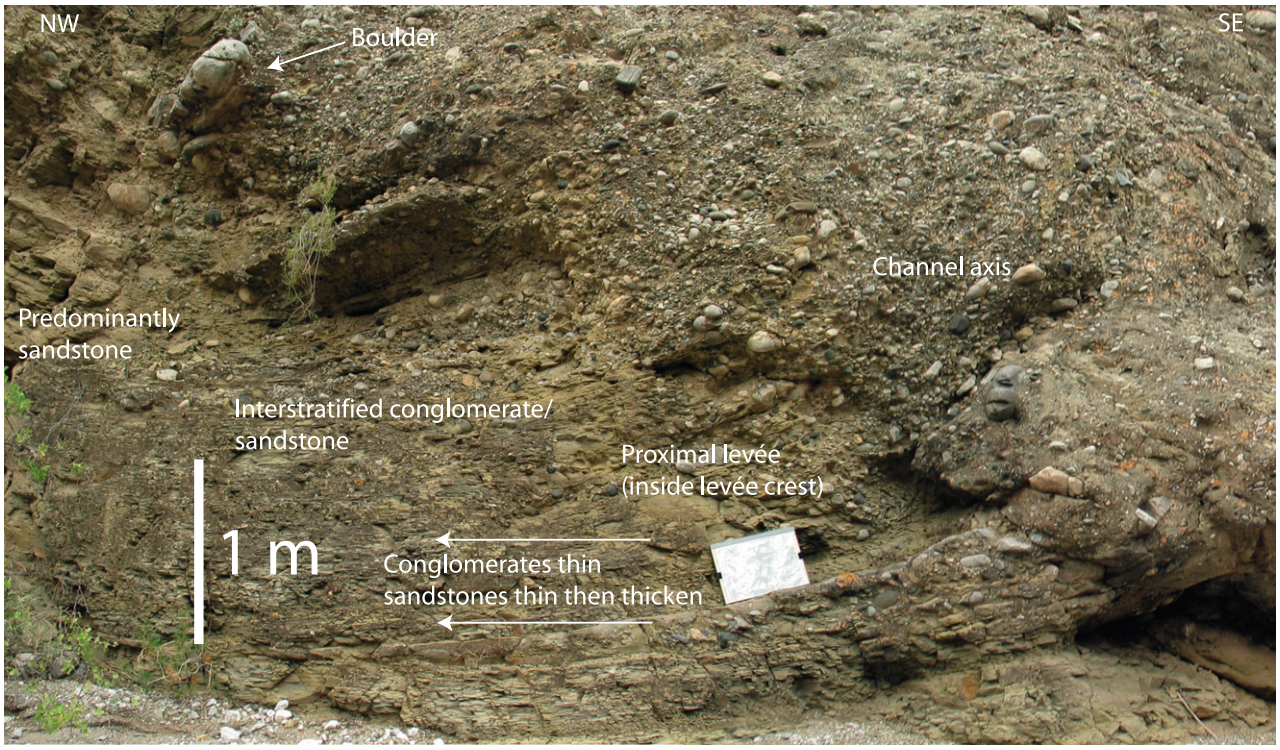

Fig. 8. Detail of the channel-margin of the channel–levée system, showing the coarse-grained channel-axis facies and the transition laterally from conglomerate to sandstone. Note how the beds fine laterally over a very short distance. Many beds can clearly be seen to thin away from the channel axis in this photograph. These beds then tend to thicken again up the inside of the levée crest, further from the channel axis.

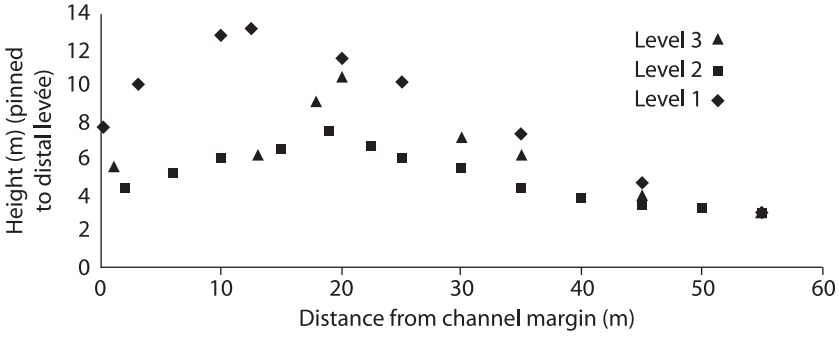

Fig. 9. Graph showing the thickness of the levée strata for the three stratigraphic levels reported here, normalized to the distal levée. Notice how the relief of the levée crest varied from 4 to 10 m relative to the distal levée.

the thicknesses does not appear to make much of a difference at this scale, and the best-fit line is very similar.

BED THICKNESS TRENDS OUTSIDE THE LEVÉE CREST

Using the same stratigraphic intervals described above outside the levée crest, the data collapse to fall on a trend best described by either a power law (Fig. 11; $R^2 = 0{\cdot}85$), exponential ($R^2 = 0{\cdot}83$) or a logarithmic relationship ($R^2 = 0{\cdot}86$). Although the fit is very good for all three, the authors prefer the power-law function for two reasons: (i) when combined with additional shallow seismic data on Pleistocene systems from the Gulf of Mexico, a power law provides a better fit (Fig. 12); and (ii) the data match very well with the thickness decay trends from levée sandstone beds in the only other well-documented outcrops exhibiting this sort of sandstone

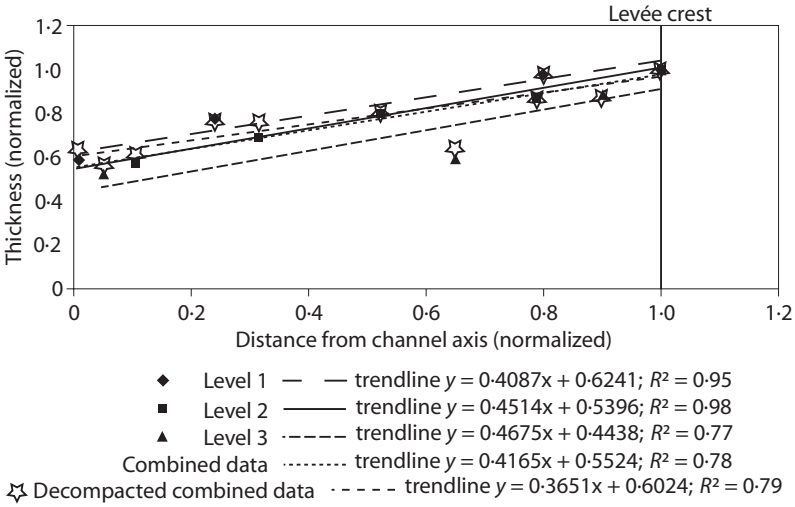

Fig. 10. Normalized thickness versus distance to the channel margin for the inner levée strata, showing the linear best-fit for each of the three individual levels, and for the grouped data, both undecompacted and decompacted.

bed thickness decay; the Canyon San Fernando channel–levée system of the Rosario Formation, Mexico (Kane *et al.*, 2007) and the Cerro Toro Formation, Chile (DeVries & Lindholm, 1994). Using the same decompaction methodology as above, the best-fit trendline to the data is still a power law (R^2 = 0·72), although the shape of the decay curve is slightly different (Fig. 11). The largest difference between the compacted and the undecompacted levée decay curves occurs in the distal levée, where the sediment is dominated by fines and thus compaction is greatest.

The present study found that the individual stratigraphic levels measured here show different best-fit lines (Figs 5 and 13); this is probably a function of minor differences in the flows, in spite of the fact that the channel-axis deposits seem to be quite homogeneous throughout the evolution of this complex. Such differences may be due to concentration of suspended sediment (producing differing rates of momentum loss as the flow moved down the levée), or due to differences in suspended grain-size distribution and thus grain settling velocity, which determine the exponent in the power law (Birman *et al.*, 2009); this would be consistent with the presence of coarser grain sizes in those beds with more rapid thickness decays. This observation suggests that the geometry of a system overall can be characterized by simple geometrical relationships, despite variations at the scale of individual beds or stratigraphic intervals.

GRAIN-SIZE TRENDS

This analysis of the grain-size trends on the levées is based on a total of ten grain-size samples, taken from two individual beds, in transects approximately perpendicular to the channel margin (Figs 5 and 6). The data can be described by either power-law (R^2 = 0·72) or logarithmic (R^2 = 0·77) decay curves; however, there is considerable scatter in the data (Fig. 14). Sorting of the grain-size samples ranges from moderate to poor, with no apparent proximal to distal trend. The grain-size decay occurs both inside and outside the levée crest (Fig. 14); the rate of decay may be different on the two sides of the levée crest, but these data are not sufficient to discriminate. The grain-size distribution in the levée sediments is predictable, where the largest grain sizes occur in the channel margin, and the mean grain size decreases in a consistent fashion away from the channel margin. The scatter in the data is probably a function of the overall size of the system. Because it is a relatively small system, a small variation in flow size through time could change the grain-size distribution substantially. To avoid this problem, the same bed was sampled for grain size, thus sampling deposits of the same flow as it moved out from the channel. Even so, any surging behaviour in the flow could affect this grain-size distribution quite markedly. Additionally, any small-scale bedforms may also affect the local grain-size distribution.

DISCUSSION

The bed thickness trends presented here outside the levée crest are consistent with trends reported in the literature from other submarine levée deposits (e.g. DeVries & Lindholm, 1994; Kane *et al.*, 2007), from experimental data (Kane *et al.*,

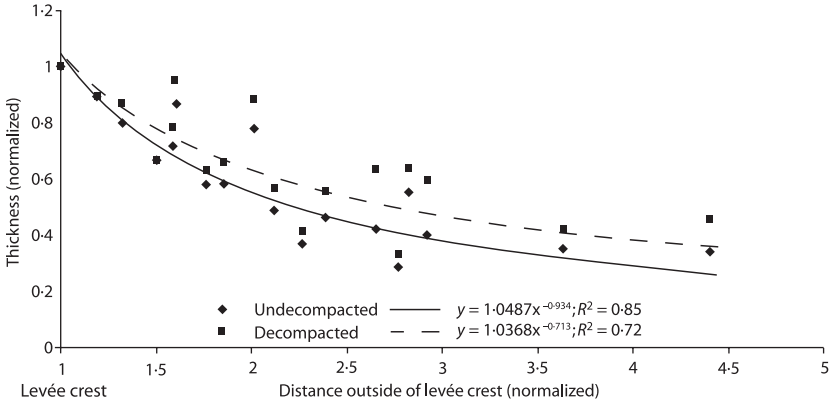

Fig. 11. Graph of the normalized thickness of the levée strata, from the levée crest to the distal levée. The thickness decay follows a power-law function away from the levée crest. The data are normalized for distance by taking the distance from the channel margin to the levée crest as one, and for thickness by taking the thickness to the levée crest as one. Undecompacted and decompacted data and best-fit trend-lines are shown.

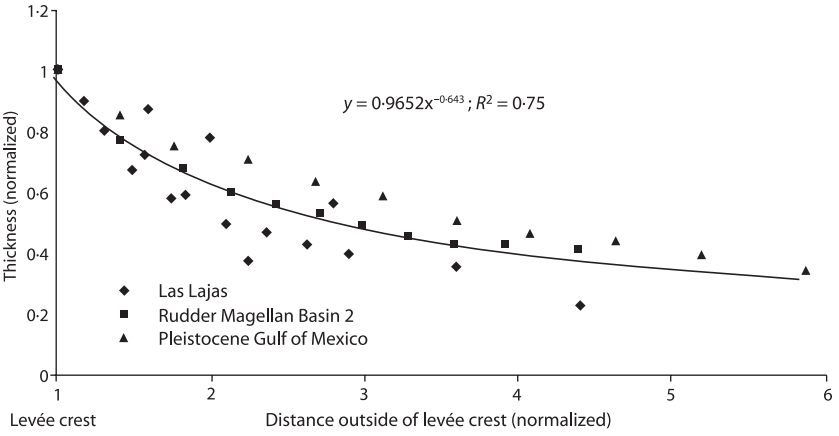

Fig. 12. Normalized levée thickness for the outcrop presented here compared with several systems from high-resolution seismic data from the sea floor of the Gulf of Mexico. Notice the excellent fit to a power-law function for all systems combined.

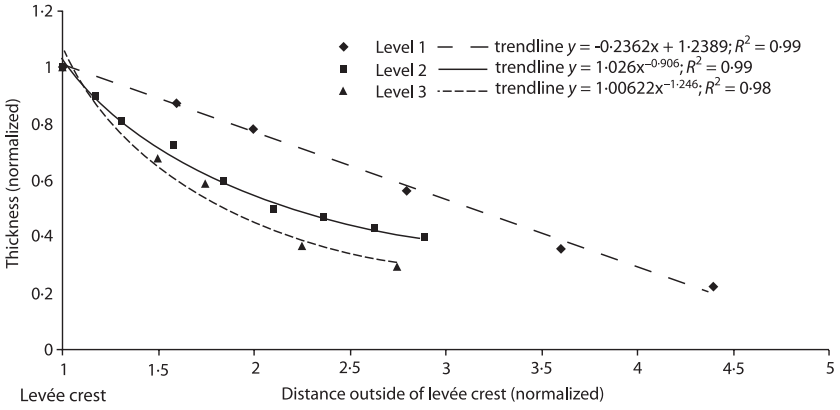

Fig. 13. Normalized levée thickness versus distance from the channel margin for the three different levels measured in the las Lajas system. Note the different equations that give a best-fit line; this is interpreted as a function of the orientation of the strata with respect to the specific flow that deposited them, and demonstrates that, although overall the levée may fit to a power law, individual architectures within the levée need not conform to this same equation.

2010) and numerical models (Birman *et al.*, 2009), as well as the thickness decays of levée packages which have been measured from published shallow seismic data (Fig. 12). Bed thickness trends inside a levée crest have not to the knowledge of the authors been previously quan-

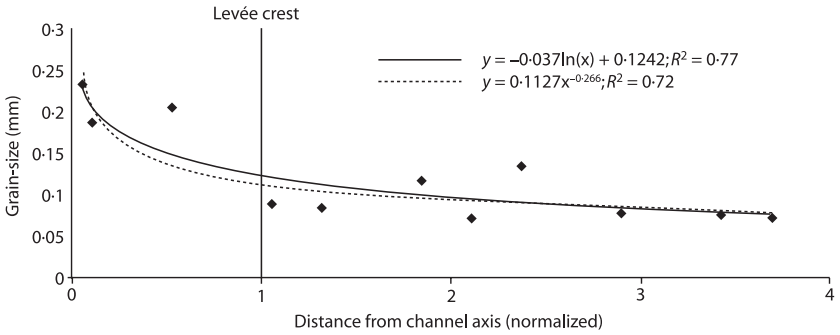

Fig. 14. Average grain-size versus distance to the channel margin (normalized), showing both a power law and a logarithmic trend-line, either of which is a relatively good fit to the data.

tified, at least in part because the temporal relationships between channel axis, margin and levée deposits cannot usually be established (Cronin *et al.*, 2000). The fact that in this setting the majority of individual event-beds are preserved from the channel margin, over the levée crest and into the distal levée allows it to be demonstrated that the channel axis, channel margin and levée beds were deposited by the same flows, thus permitting a process analysis not possible with other datasets. Important questions which can be addressed with this dataset include: (i) what process controls bed thinning from the channel axis to the channel margin (as defined above); (ii) is the same process responsible for bed thickening from the channel margin to the levée crest that is responsible for bed thinning away from the levée crest; and (iii) what control, if any, does the topography of the levée crest have on grain-size trends?

There is strong evidence for tractional transport of the sediment, both in the channel margin area and at the levée crest, including (in the channel margin) currents strong enough to transport pebbles and cobbles as bedload, whereas this evidence is absent in the channel axis, where deposits are quite chaotic (Fig. 15). This lateral change is probably reflective of the actual transport processes rather than merely giving a shapshot of the instant of deposition or of post-depositional reworking, due to the complete dominance of each deposit type in the channel axis and the channel margin. These differences reflect a lateral change in the nature of the depositing flows from relatively cohesive, probably laminar, flows in the channel axis to more dilute, turbulence-supported suspensions on the channel margin and overtopping the levée. Furthermore, this change occurs on a spatial scale of a few metres laterally and tens of centimetres vertically, and there is direct palaeocurrent evidence that the flows in the channel margin originated in the channel axis. The most likely mechanism for this rapid lateral change was the existence of cogenetic laminar and turbulent flow. In this hypothesis, a dense, probably laminar, flow would have been present in the channel axis, overlain by a turbulent flow that extended over the channel margin and levées. The co-existence of these two flow types may be due to the partial transformation of the parent flow, at some point upstream, probably by fluid entrainment (Fisher, 1983; Waltham, 2004). This fluid entrainment was probably a continuous process occurring across the boundaries of the laminar part of the flow. Transformations from laminar to turbulent flows have been shown to decrease either the capacity or the competence of the flows by slowing them (Britter & Linden, 1980). Similar flow transformations have been produced in experiments on quite small-scales (Mohrig & Marr, 2003; Felix & Peakall, 2006); the scale and degree of transformation from a laminar to a turbulent flow was shown to depend strongly on the initial viscosity and density of the flow (Felix & Peakall, 2006) or, for similar viscosity flows, on the shear strength to dynamic stress ratio (Mohrig & Marr, 2003). For relatively fluid and dilute debris flows, the transformation to turbidity currents was quite abrupt and complete, although there was a wide range of flow rheologies produced in these experiments (Felix & Peakall, 2006). The ability for fluid to become entrained in the flow appears to be a critical factor in this transformation. Alternatively, the opposite sort of transformation may have occurred, such that a single, more homogeneous dense suspension may have become partitioned downstream, by collapse of the turbulent support, into a highly concentrated (perhaps laminar) basal layer, and a more dilute overriding turbidity current, much in the

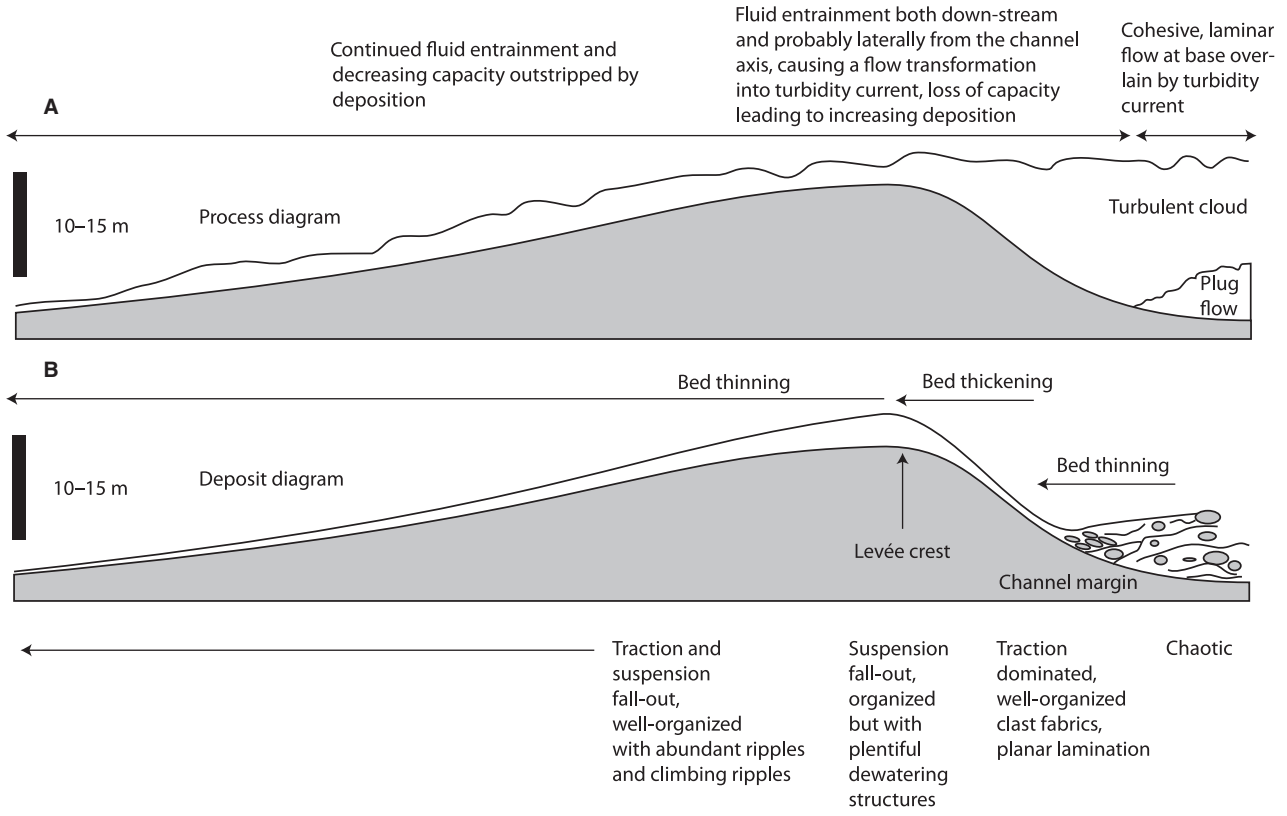

Fig. 15. Cartoons showing a channel to levée transect, perpendicular to the palaeocurrent direction in the channel axis. (A) Shows a snapshot of the process interpretation, with a laminar debris flow in the channel axis laterally and vertically overridden by a turbidity current probably generated from the debris flow through the process of fluid entrainment. (B) The resultant deposit, showing a lateral thinning from the channel axis to the margin, a thickening to a maximum at the levée crest, and a thinning outward from there.

way that dense pyroclastic flows may transform (Fisher, 1983).

Fluid entrainment within the turbulent flow may also be the simplest explanation for the bed thickening patterns observed from the channel margin to the levée crest; as fluid is entrained, both the capacity and the competence of the flow decreases, causing more rapid sedimentation (Birman *et al.*, 2009; Kane *et al.*, 2010). Alternatively, the thinning then thickening patterns from the channel axis to margin to levée crest could simply relate to the duration of sedimentation. At the levée crest, deposition of sediment may have occurred over the entire duration of any given flow, while bypass dominated further in toward the channel margin. As the flow subsequently waned, deposition would have begun to dominate on the channel margin and finally in the channel axis. The question remains as to why beds initially thin from the channel axis toward the margin and then thicken. If the duration of sedimentation hypothesis is correct, this relationship could be because the flow in the channel axis is laminar, it may leave a slightly thicker deposit than on the proximal channel margin. If the capacity driven hypothesis is correct, this thinning then thickening pattern could relate to the flow transformation from laminar to turbulent at the channel-axis/margin boundary. This change to turbulence may initially suppress sedimentation by providing more kinetic energy to the flow to suspend particles.

Bed thinning outside the levée crest, on the other hand, could be explained by either capacity-driven or competence-driven sedimentation. Competence-driven sedimentation has been shown to result in beds that thin exponentially away from the source (Gladstone *et al.*, 1998; De Rooij & Dalziel, 2009; Kane *et al.*, 2010) although, as Kane *et al.* (2010) point out, fluid entrainment on steeper levée backslopes may result in power-law rather than exponential bed thickness decays (Birman *et al.*, 2009). The present authors favour competence-driven sedimentation because tractional structures, such as ripple cross-lamination and planar lamination, are common in the channel margin and the levée.

From the grain-size data (Fig. 14), the topography of the levée crest appears to only exert a minor control on grain-size trends in the more distal channel margin and levée sediments. Because these sediments are made up of grain populations that were originally in suspension, their distribution was controlled largely by the interaction between the levée topography and the part of the suspension cloud that carried sand. Topography is a major control, however, on the distribution of very large grain sizes (gravel) which were probably never in suspension; the levée topography formed a complete barrier to the relatively thin bed-load layer, or the high-concentration (perhaps laminar) non-Newtonian component of the flow that dominated near-bed channel axis transport.

The channel–levée system presented here is very small, and sits in a rather unusual setting, compared with the majority of channel–levée systems reported from the literature (DeVries & Lindholm, 1994; Browne & Slatt, 2002; Hickson & Lowe, 2002; Kane *et al.*, 2007). Although the results presented here suggest that the levée beds themselves, from the levée crest outward, are built by the same or very similar processes to those in other subaqueous levées, there are some important differences between this small-scale, highly aggradational channel–levée system and others reported in the literature. Firstly, in this case it can be demonstrated that the channel axis and margin were coeval with the levée beds, whereas in most channel–levée systems in outcrop and in the subsurface this is not the case – usually erosion surfaces separate the channel axis from the levée and, therefore, a temporal relationship cannot be firmly established (Coleman, 2000; Cronin *et al.*, 2000; Kane *et al.*, 2007; Kane & Hodgson, 2011). Secondly, this system was pro-glacial, and probably received a high sediment supply with rapid aggradation and progradation rates, and probably was deposited in only hundreds to thousands of years (Dykstra *et al.*, 2007b). Thirdly, this system was deposited in only a few tens of metres of water depth and only hundreds of metres down-valley from its sediment supply (the glacier), and possibly on a relatively steep slope (Dykstra *et al.*, 2007b). Finally, the water salinities in this system may have been quite low, due to the significant input of fresh water from the valley glacier (Dykstra *et al.*, 2006). What difference these last few factors make is a matter still up for debate, but certainly the high aggradation rates would suppress the development of any major erosion surfaces, and may be a major factor in the preservation of beds from channel axis to levée.

CONCLUSIONS

These observations lead to several general conclusions regarding sub-aqueous levée formation and sediment gravity-flow processes, including:

1 Levée thickness trends both inside and outside the levée crest seem to be genetically linked to processes that generated deposits within the channel, at least in this case.

2 Bed-scale changes in thickness are the primary control on overall thickness changes in this levée, which can be seen both at the level of individual beds and of entire stratigraphic packages (consisting of several beds, and including the entire grain-size range).

3 The outer levée exhibits a thickness decay best described by power-law functions, while inside the levée crest, beds thin initially and then thicken linearly away from the channel axis up to the levée crest.

4 Grain-size distributions on this levée from the channel outward are equally well-described by either logarithmic or power-law decays.

5 From the channel axis to the channel margin there is a transition from chaotic debris-flow deposits to well-organized turbidite deposits. This transition occurs over only a few metres laterally, and is probably due to the upstream generation of two co-existing flows by fluid entrainment along the boundaries of the axial, laminar flow, or by the collapse of a single dense suspension to form a dense basal (probably laminar) depositional layer and an overriding turbidity current.

6 There is a remarkable consistency between the thickness decays in this system and decays in published seismic data, even though these data are from a much smaller scale system (in a confined basin setting) than those published accounts on large-scale, deep marine systems. This architectural consistency suggests that the main control on levée geometry is provided by flow processes, rather than local controls, such as basin setting, morphology, salinity or grain-size distribution.

ACKNOWLEDGEMENTS

We acknowledge the contributions of our research sponsors, including Anadarko Petroleum, BG-Group, BHP Billiton-Americas and Statoil. Fieldwork was aided by Diego Rodriguez, and

facilitated by Dr Silvio Peralta and the Universidad Nacional de San Juan, Argentina. This paper benefitted from discussions with Ian Kane. Excellent reviews were provided by Ian Kane and one anonymous reviewer.

REFERENCES

Beaubouef, R.T. (2004) Deep-water leveed channel complexes of the Cerro Toro Formation, Upper Cretaceous, southern Chile. *Am. Assoc. Petrol. Geol. Bull.*, **88,** 1471–1500.

Beresi, M.S. and **Bordonaro, C.L.** (1985) La formacion San Juan en la Quebrada de las Lajas, Sierra Chica de Zonda, Provincia de San Juan. *Actas Congr. Geol. Argentino*, **9,** 95–107 (Asociacion Geologica Argentina, Buenos Aires).

Birman, V.K., Meiburg, E. and **Kneller, B.** (2009) The shape of submarine levees: exponential or power law? *J. Fluid Mech.*, **619,** 367–376.

Bond, G.C. and **Kominz, M.A.** (1984) Construction of tectonic subsidence curves for the early Paleozoic miogeocline, southern Canadian Rocky Mountains: Implications for subsidence mechanisms, age of breakup, and crustal thinning. *Bull. Geol. Soc. Am.*, **95,** 155.

Bonnecaze, R.T., Huppert, H.E. and **Lister, J.R.** (1993) Particle-driven gravity currents. *J. Fluid Mech.*, **250,** 339–369.

Britter, R.E. and **Linden, P.F.** (1980) The motion of the front of a gravity current travelling down an incline. *J. Fluid Mech.*, **99,** 531–543.

Browne, G.H. and **Slatt, R.M.** (2002) Outcrop and behind-outcrop characterization of a late Miocene slope fan system, Mt. Messenger Formation, New Zealand. *AAPG Bull.*, **86,** 841–862.

Chough, S. and **Hesse, R.** (1980) The Northwest Atlantic Mid-Ocean Channel of the Labrador Sea; III, Head spill vs. body spill deposits from turbidity currents on natural levees. *J. Sedim. Res.*, **50,** 227.

Clemenceau, G.R., Colbert, J. and **Edens, D.** (2000) Production Results from Levee-Overbank Turbidite Sands at Ram/Powell Field, Deepwater Gulf of Mexico. In: *GCSSEPM Foundation 20th Annual Research Conference* (Eds P. Weimer, R.M. Slatt, J. Coleman, N.C. Rosen, H. Nelson, A.H. Bouma, M.J. Styzen and D.T. Lawrence), pp. 241–251. GCSSEPM, Houston, TX.

Coleman, J.L. (2000) Reassessment of the Cerro Toro (Chile) Sandstones in View of Channel–Levee–Overbank Reservoir Continuity Issues. In: *Deep Water Reservoirs of the World* (Eds P. Weimer, R.M. Slatt, J. Coleman, N.C. Rosen, H. Nelson, A.H. Bouma, M.J. Styzen and D.T. Lawrence), vol. 20, pp. 252–262. GCSSEPM Foundation, Houston, TX.

Cronin, B.T., Hurst, A., Celik, H. and **Turkmen, I.** (2000) Superb exposure of a channel, levee and overbank complex in an ancient deep-water slope environment. *Sedim. Geol.*, **132,** 205–216.

Damuth, J.E., Flood, R.D., Kowsmann, R.O., Belderson, R.H. and **Gorini, M.A.** (1988) Anatomy and growth pattern of Amazon deep-sea fan as revealed by long-range side-scan sonar (GLORIA) and high-resolution seismic studies. *AAPG Bull.*, **72,** 885.

De Rooij, F. and **Dalziel, S.B.** (2009) Time- and space-resolved measurements of deposition under turbidity currents. In: *Particulate Gravity Currents* (Eds W.D. McCaffrey, B.C. Kneller and J. Peakall) Blackwell Publishing, Oxford, **31,** 207–215.

DeVries, M.B. and **Lindholm, R.M.** (1994) Internal architecture of a channel–levee complex, Cerro Toro Formation, southern Chile. In: *Submarine Fans and Turbidite Systems: Sequence Stratigraphy, Reservoir Architecture, and Production Characteristics* (Eds P. Weimer, A. Bouma and B.F. Perkins), vol. 14, pp. 105–114. GCSSEPM, Houston, TX.

Dykstra, M. (2005) *Dynamics of Sediment Mass-Transport from the Shelf to the Deep Sea*. PhD thesis, University of California, Santa Barbara, Santa Barbara, 152 pp.

Dykstra, M., Kneller, B. and **Milana, J.-P.** (2006) Deglacial and postglacial sedimentary architecture in a deeply incised paleovalley-paleofjord – The Pennsylvanian (late Carboniferous) Jejenes Formation, San Juan, Argentina. *GSA Bull.*, **118,** 913–937.

Dykstra, M., Kneller, B. and **Milana, J.P.** (2007a) A high-resolution record of deepwater processes in a confined paleofjord, Quebrada de las Lajas, Argentina. In: *Atlas of Deepwater Outcrops; CD ROM* (Eds T.H. Nilsen, R.D. Shew, G.S. Steffens and J.R.J. Studlick), *AAPG Stud. Geol.*, **56,** p. 19. AAPG and Shell Exploration and Production, Tulsa, OK.

Dykstra, M., Kneller, B. and **Milana, J.P.** (2007b) Quebrada de las Lajas: A High Resolution Record of Deep Water Processes in a Confined Paleovalley. In: *Atlas of Deepwater Outcrops* (Eds T.H. Nilsen, R.D. Shew, G.S. Steffens and J.R.J. Studlick), *AAPG Stud. Geol.*, **56,** pp. 42–44. AAPG and Shell Exploration and Production, Tulsa, OK.

Felix, M. (2002) Flow structure of turbidity currents. *Sedimentology*, **49,** 397–419.

Felix, M. and **Peakall, J.** (2006) Transformation of debris flows into turbidity currents: mechanisms inferred from laboratory experiments. *Sedimentology*, **53,** 107–123.

Fernández Seveso, F. and **Tankard, A.J.** (1995) Tectonics and stratigraphy of the Late Paleozoic Paganzo Basin of Western Argentina and its Regional Implications. In: *Petroleum Basins of South America* (Eds A.J. Tankard, S. Suarez and H.J. Welsink), *AAPG Memoir*, **62,** pp. 285–301. AAPG.

Fisher, R.V. (1983) Flow transformations in sediment gravity flows. *Geology*, **11,** 273.

Fleisher, P.J., Bailey, P.K. and **Cadwell, D.H.** (2003) A decade of sedimentation in ice-contact, proglacial lakes, Bering Glacier, AK. *Sedim. Geol.*, **160,** 309–324.

Gladstone, C., Phillips, J.C. and **Sparks, R.S.J.** (1998) Experiments on bidisperse, constant-volume gravity currents: propagation and sediment deposition. *Sedimentology*, **45,** 833–843.

Hickson, T.A. and **Lowe, D.R.** (2002) Facies architecture of a submarine fan channel–levee complex: the Juniper Ridge Conglomerate, Coalinga, California. *Sedimentology*, **49,** 335–362.

Hubbard, S.M., Romans, B.W. and **Graham, S.A.** (2008) Deep-water foreland basin deposits of the Cerro Toro Formation, Magallanes basin, Chile: architectural elements of a sinuous basin axial channel belt. *Sedimentology*, **55,** 1333–1359.

Iverson, R.M. (1997) The physics of debris flows. *Rev. Geophys.*, **35,** 245–296.

Kane, I.A. (2007) *Architecture and Sedimentology of Submarine Channel–Levee Systems: Insights from the Upper Cretaceous Rosario Formation, Baja California, Mexico, and from Laboratory Experiments*, University of Leeds, Leeds, 340 pp.

Kane, I.A. and **Hodgson, D.M.** (2011) Sedimentological criteria to differentiate submarine channel levee subenvironments: exhumed examples from the Rosario Fm.(Upper Cretaceous) of Baja California, Mexico, and the Fort Brown Fm.(Permian), Karoo Basin, S. Africa. *Mar. Petrol. Geol.*, **28,** 807–823.

Kane, I.A., Kneller, B.C., Dykstra, M., Kassem, A. and **McCaffrey, W.D.** (2007) Anatomy of a submarine channel–levee: An example from Upper Cretaceous slope sediments, Rosario Formation, Baja California, Mexico. *Mar. Petrol. Geol.*, **24,** 540–563.

Kane, I.A., McCaffrey, W.D., Peakall, J. and **Kneller, B.C.** (2010) Submarine channel levee shape and sediment waves from physical experiments. *Sedim. Geol.*, **223,** 75–85.

Keller, M. (1999) Argentine Precordillera: Sedimentary and Plate Tectonic History of a Laurentian Crustal Fragment in South America. In: *Argentine Precordillera: Sedimentary and Plate Tectonic History of a Laurentian Crustal Fragment in South America* (Ed. M. Keller), Geological Society of America Special Paper 341, pp. 131. Geological Society of America, Boulder, CO.

Kneller, B.C. (1995) Beyond the turbidite paradigm: Physical models for deposition of turbidites and their implications for reservoir prediction. In: *Characterisation of Deep Marine Clastic Systems*. Special Publication 94, pp. 29–46. Geological Society, London.

Kneller, B. (2003) The influence of flow parameters on turbidite slope channel architecture. *Mar. Petrol. Geol.*, **20,** 901–910.

Kneller, B. and **Buckee, C.** (2000) The structure and fluid mechanics of turbidity currents; a review of some recent studies and their geological implications. *Sedimentology*, **47**(Suppl. 1)**,** 62–94.

Kneller, B., Milana, J.P., Buckee, C. and **al Ja'aidi, O.** (2004) A depositional record of deglaciation in a paleofjord (Late Carboniferous [Pennsylvanian] of San Juan Province, Argentina): the role of catastrophic sedimentation. *GSA Bull.*, **116,** 348–367.

Limarino, C.O., Cesari, S.N., Net, L.I., Marenssi, S.A., Gutierrez, R.P. and **Tripaldi, A.** (2002) The Upper Carboniferous postglacial transgression in the Paganzo and Rio Blanco basins (northwestern Argentina): facies and stratigraphic significance. *J. South Am. Earth Sci.*, **15,** 445–460.

López-Gamundí, O.R., Limarino, C.O. and **Cesari, S.N.** (1992) Late Paleozoic paleoclimatology of central west Argentina. *Palaeogeogr. Palaeoclimatol. Palaeoecol.*, **91,** 305–329.

Mackiewicz, N.E., Powell, R.D., Carlson, P.R. and **Molnia, B.F.** (1984) Interlaminated ice-proximal glacimarine sediments in Muir Inlet, Alaska. *Mar. Geol.*, **57,** 113–147.

Milana, J.P. and **Bercowski, F**. (1990) Facies y Geometría de depósitos glaciales en un paleovalle Carbonífero de Precordillera Central, San Juan, Argentina: 3ª Reunión Argentina de Sedimentología, San Juan, Actas, pp. 199–204.

Mohrig, D. and **Buttles, J.** (2007) Deep turbidity currents in shallow channels. *Geology*, **35,** 155–158.

Mohrig, D. and **Marr, J.G.** (2003) Constraining the efficiency of turbidity current generation from submarine debris flows and slides using laboratory experiments. *Mar. Petrol. Geol.*, **20,** 883–899.

Normark, W. (1978) Fan valleys, channels, and depositional lobes on modern submarine fans: characters for recognition of sandy turbidite environments. *Am. Assoc. Petrol. Geol. Bull.*, **62,** 912–931.

Pazos, P.J. (2002) The Late Carboniferous glacial to postglacial transition; facies and sequence stratigraphy, western Paganzo Basin, Argentina. *Gondwana Res.*, **5,** 467–487.

Peakall, J., McCaffrey, B. and **Kneller, B.** (2000) A process model for the evolution, morphology, and architecture of sinuous submarine channels. *J. Sedim. Res.*, **70,** 434–448.

Ramos, V.A. (1988) The tectonics of central Andes; 30°-33° S latitude. In: *Processes in Continental Lithosphere Deformation* (Eds S. Clark and D. Burchfiel), *GSA Special Paper*, **218,** pp. 31–54. GSA, Boulder.

Salfity, J.A. and **Gorustovich, S.A.** (1983) Paleogeografía de la Cuenca de Paganzo (Paleozoico Superior). *Rev. Asoc. Geol. Argentina*, **38,** 437–453.

Skene, K.I., Piper, D.J.W. and **Hill, P.S.** (2002) Quantitative analysis of variations in depositional sequence thickness from submarine channel levees. *Sedimentology*, **49,** 1411–1430.

Waltham, D. (2004) Flow transformations in particulate gravity currents. *J. Sedim. Res.*, **74,** 129.

Manuscript received 9 March 2010; revision accepted 20 May 2011